Photosynthesis Research
https://doi.org/10.1007/s11120-024-01084-8

RESEARCH

On the simulation and interpretation of substrate-water exchange experiments in photosynthetic water oxidation

Petko Chernev[1] · **A. Orkun Aydin**[1] · **Johannes Messinger**[1]

Received: 3 November 2023 / Accepted: 1 February 2024

Abstract

Water oxidation by photosystem II (PSII) sustains most life on Earth, but the molecular mechanism of this unique process remains controversial. The ongoing identification of the binding sites and modes of the two water-derived substrate oxygens ('substrate waters') in the various intermediates (S_i states, $i = 0, 1, 2, 3, 4$) that the water-splitting tetra-manganese calcium penta-oxygen (Mn_4CaO_5) cluster attains during the reaction cycle provides central information towards resolving the unique chemistry of biological water oxidation. Mass spectrometric measurements of single- and double-labeled dioxygen species after various incubation times of PSII with $H_2{}^{18}O$ provide insight into the substrate binding modes and sites via determination of exchange rates. Such experiments have revealed that the two substrate waters exchange with different rates that vary independently with the S_i state and are hence referred to as the fast (W_f) and the slow (W_S) substrate waters. New insight for the molecular interpretation of these rates arises from our recent finding that in the S_2 state, under special experimental conditions, two different rates of W_S exchange are observed that appear to correlate with the high spin and low spin conformations of the Mn_4CaO_5 cluster. Here, we reexamine and unite various proposed methods for extracting and assigning rate constants from this recent data set. The analysis results in a molecular model for substrate-water binding and exchange that reconciles the expected non-exchangeability of the central oxo bridge O5 when located between two Mn(IV) ions with the experimental and theoretical assignment of O5 as W_S in all S states. The analysis also excludes other published proposals for explaining the water exchange kinetics.

Keywords Photosystem II · Oxygen-evolving complex · Mechanism of water oxidation · Membrane inlet mass spectrometry (MIMS) · Substrate-water exchange

Abbreviations

EPR	Electron paramagnetic resonance
DFT	Density functional theory
E	Conformational state of enzyme
k_c	Rate of equilibration between HS and LS state
k_f, k_S	Fast and slow rate for substrate-water exchange
k^*	Apparent rate constant
HS, LS	High spin, low spin
MIMS	Membrane inlet mass spectrometry
$Mn_4CaO_{5/6}$	Inorganic cofactor of the OEC with 5 (S_0–S_2) or 6 (S_3, S_4) oxo bridges
OEC	Oxygen-evolving complex: functional unit of PSII that catalyzes water oxidation
O5	Central oxygen bridge of the $Mn_4CaO_{5/6}$ cluster
PSII	Photosystem II
S_i states	Oxidation states of the $Mn_4CaO_{5/6}$ cluster ($i = 0, 1, 2, 3, 4$)
W_f, W_S	Fast and slowly exchanging substrate water bound to the $Mn_4CaO_{5/6}$ cluster
W_N	New water added to the Mn_4CaO_5 cluster during the $S_2 \rightarrow S_3$ transition
W1–W4	Terminal water ligands of the OEC
^{34}Y, ^{36}Y	Oxygen yield at mass-to-charge ratio 34 and 36
XFEL	X-ray free electron laser
α_{in}, α_f	Initial and final ^{18}O isotope enrichment of the buffer

✉ Johannes Messinger
johannes.messinger@kemi.uu.se

[1] Molecular Biomimetics, Department of Chemistry – Ångström Laboratory, 75120 Uppsala, Sweden

Published online: 21 March 2024

Introduction

Photosystem II (PSII) catalyzes the oxidation of water into molecular oxygen and protons. The reaction happens at the Mn_4CaO_5 cluster (Fig. 1A) in the oxygen-evolving complex (OEC) of PSII, which is oxidized stepwise within a catalytic cycle that is driven by light-induced charge separations in the reaction center of PSII. Thus, the OEC is going through five intermediate states, S_0 through S_4, where the subscript indicates the number of stored oxidizing equivalents (Fig. 1B) (Kok et al. 1970). Molecular oxygen is released in the transition of the highly reactive S_4 state to S_0 in which also one substrate water binds, while the second substrate water is inserted into the cluster during the $S_2 \rightarrow S_3$ transition (Dau et al. 2010; Pantazis 2018; Kern et al. 2018; Lubitz et al. 2019; Junge 2019; Suga et al. 2019; Ibrahim et al. 2020; Yamaguchi et al. 2022b; Shevela et al. 2023). High-resolution structures have been reported first for the dark-stable S_1 state (Umena et al. 2011; Suga et al. 2015; Tanaka et al. 2017; Young et al. 2016), and recently also for the S_2, S_3, and S_0 states (Kern et al. 2018; Suga et al. 2017) and several time points during the $S_3 \rightarrow S_4 \rightarrow S_0$ transition (Bhowmick et al. 2023).

Despite the great advancement in the structural resolution of PSII in its reaction cycle, the mechanism of the O–O bond formation remains controversial (Vinyard et al. 2013, 2017; Li and Siegbahn 2015; Lubitz et al. 2019; Yamaguchi et al. 2022a; Greife et al. 2023; Bhowmick et al. 2023; Shevela et al. 2023). An important step towards resolving some of the open questions would be to identify the two substrate waters in all the S states. Presently, the only technique that can provide a unique signature for the substrate water molecules is time-resolved membrane inlet mass spectrometry (TR-MIMS) in combination with $H_2{}^{16}O/H_2{}^{18}O$ exchange (Messinger et al. 1995; Messinger 2004; Hillier and Wydrzynski 2008; Cox and Messinger 2013). In this method, $H_2{}^{18}O$ is rapidly injected into a PSII

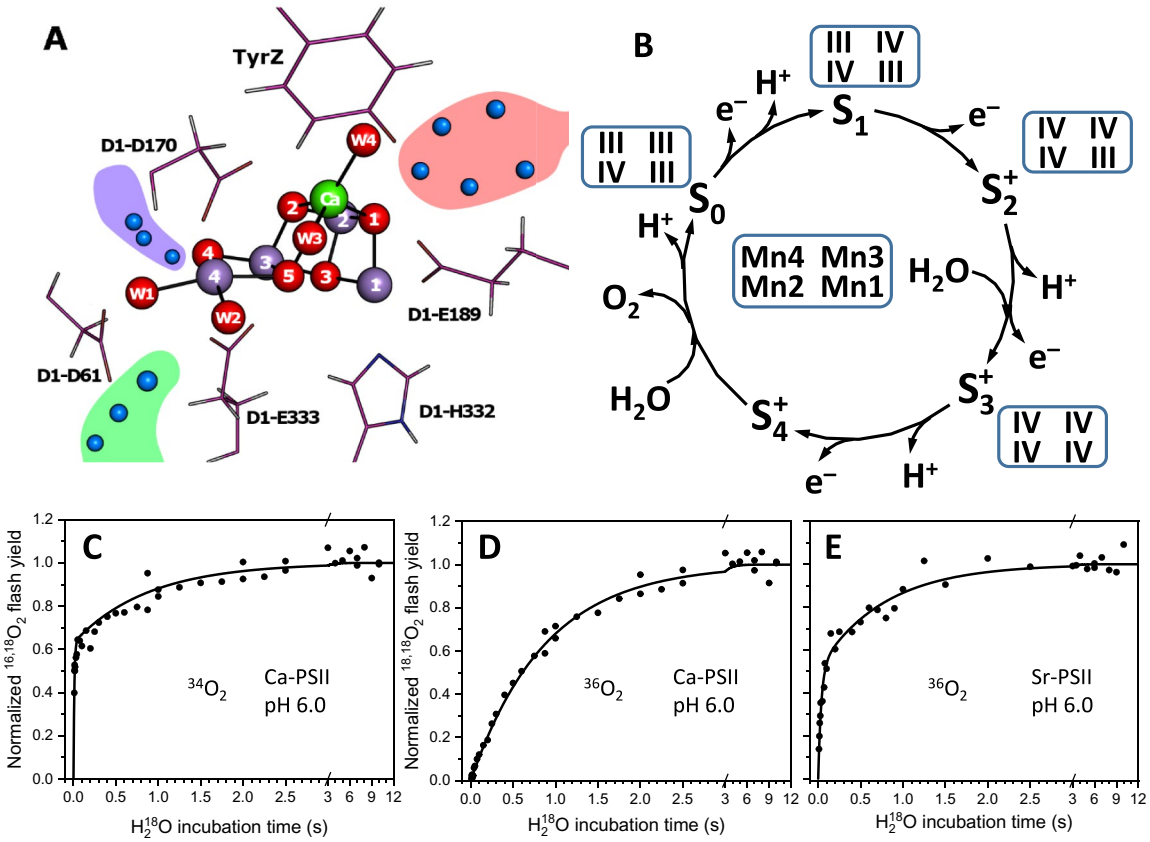

Fig. 1 The oxygen-evolving complex of PSII, its reaction cycle, and substrate-water exchange experiments. **A** Structure of the Mn_4CaO_5 cluster and its surrounding (PDB: 7RF1). Manganese is shown in magenta, oxygen in red, calcium in green, water molecules around the active site in blue. Water-filled channels are represented with red (O1 channel), blue (O4 channel), and green (Cl1 channel) areas. **B** S state cycle of the Mn cluster. The formal oxidation states of the four Mn atoms in the four quasi-stable states are given in the boxes next to the state. **C**, **D** TR-MIMS measurements of the water exchange in the S_2 state of Ca-PSII showing the single ^{18}O-labeled (**C**) and double-labeled (**D**) O_2 yield at pH 6. **E** double-labeled O_2 yield of Sr-PSII. Points in **C**–**E** show individual experimental data points, and lines show exponential fits; redrawn from Ref. de Lichtenberg and Messinger (2020)

sample and the isotopic composition of the O_2 produced by flash illumination after various incubation times is measured in order to determine the exchange rates of the two substrate waters.

The TR-MIMS measurements reveal a fast-exchanging (W_f) and a slowly exchanging (W_S) substrate water. The exchange of W_S can be resolved in all quasi-stable S states and usually happens on time scales from tens of milliseconds (S_0 state) through seconds (S_2 and S_3) to tens of seconds (S_1). The half-time of W_f exchange in the S_2 and S_3 states is also resolvable in the TR-MIMS measurements, at around 7 to 25 ms, while in the S_0 and S_1 states W_f exchanges faster than it can be resolved with this method (Hillier et al. 1998; Hillier and Wydrzynski 2000; Nilsson et al. 2014a; Cox and Messinger 2013). The biphasic behavior of the single ^{18}O-labeled O_2 yield (denoted ^{34}Y) reflects the distinct exchange kinetics of the two substrate waters (Fig. 1C), while the yield of the double-labeled O_2 (^{36}Y) rises usually monophasic and is mostly determined by the exchange of W_s (Fig. 1D). Therefore, the TR-MIMS data can be analyzed by fitting a single-exponential curve to the ^{36}Y-vs-time plot, while ^{34}Y requires two exponential components (Messinger et al. 1995; Hillier and Wydrzynski 2000):

$$^{34}\mathrm{Y} = a\left(1 - e^{-k_f t}\right) + (1-a)\left(1 - e^{-k_s t}\right)$$

$$^{36}\mathrm{Y} = 1 - e^{-k_s t} \tag{1}$$

These equations describe a system with pseudo-first-order kinetics, where exchange happens at two independent sites with apparent rate constants k_f and k_s, under the condition that $k_f \gg k_s$. The parameter a describes the exponential component proportions of the fast and slow exchange in the ^{34}Y data, and it can be shown (Messinger et al. 1995) that a should be a function of the isotope contents of the bulk water in the sample:

$$a = \frac{\alpha_f\left(1-\alpha_{in}\right) + \alpha_{in}\left(1-\alpha_f\right)}{2\alpha_f\left(1-\alpha_f\right)}, \tag{2}$$

where α_{in} and α_f are the initial and final $H_2{}^{18}O$ enrichment correspondingly; a is approximately equal to $0.5/(1-\alpha_f)$ if the initial enrichment (estimated to be around 0.7% in these experiments) is ignored.

The S_2 state can exist in at least two different conformations, one having an EPR signal centered at $g = 2.0$ (low spin, LS) and the other at 4.1 (high spin, HS) (Dismukes and Siderer 1981; Zimmermann and Rutherford 1984; Kim et al. 1992). Only the $g = 2.0$ conformation (Fig. 1A) is observed in untreated cyanobacterial PSII in serial crystallography experiments at room temperature (Kern et al. 2018; Li et al. 2021), but EPR experiments reveal that by Ca/Sr exchange and/or high pH a HS conformation can be induced that occurs at $g = 4.8$–4.9, indicating that it may differ in structure compared to $S_2{}^{HS}$ of plant PSII (Boussac et al. 2018). At least three different conformations have been suggested for the $Mn_4CaO_{5/6}$ cluster in the $S_2{}^{HS}$ state (Fig. 2), which all were shown by DFT calculations to give the $S = 5/2$ spin state (Pantazis et al. 2012; Corry and O'Malley 2019; Pushkar et al. 2019), while models B and C were also favorably compared to x-ray spectroscopy results of $S_2{}^{HS}$ (Pushkar et al. 2019; Chatterjee et al. 2019). It is noted that the three proposals are not mutually exclusive and that the ability of the Mn_4CaO_5 cluster to transiently attain additional conformations in the S_2 state forms the basis of the proposal for exchanging the central O5 bridge (Siegbahn 2013).

The HS and LS conformations may exhibit different substrate-water exchange kinetics, and if a sample contains significant (> 10%) fractions of both conformations, then Eq. (1) may not be a suitable description of the system. In that case, an additional kinetic component may be observed in the ^{34}Y and ^{36}Y signals, and has been fitted by the following expressions (de Lichtenberg and Messinger 2020):

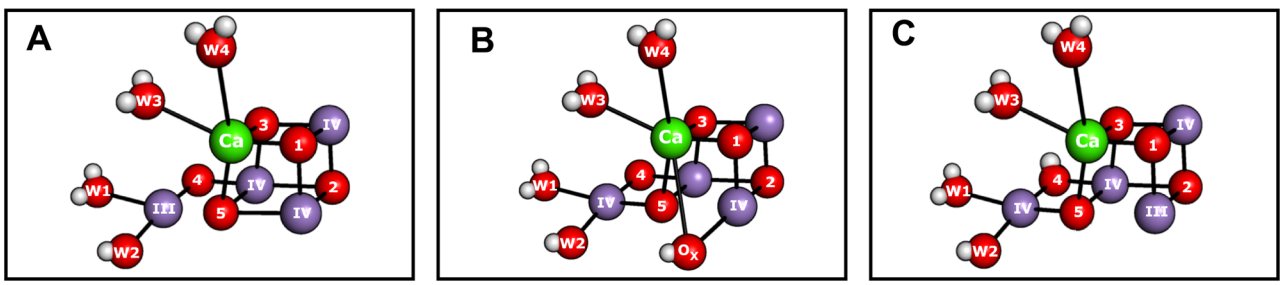

Fig. 2 Proposals for high spin ($g \geq 4.1$) conformation of the OEC in S_2 state. **A** Closed cubane model in which the 'dangling' Mn4 is a pentacoordinate Mn(III) ion (Pantazis et al. 2012; Isobe et al. 2012; Bovi et al. 2013); **B** early water binding between Mn1 and Ca (Pushkar et al. 2019; de Lichtenberg and Messinger 2020) in which Mn2 or Mn3 maybe the only Mn(III) (Pushkar et al. 2019); **C** proton isomer of the open cubane conformation in which, compared to $S_2{}^{LS}$, a proton is moved from W1 to O4 (Corry and O'Malley 2019). Manganese atoms are shown in magenta, calcium in green, and oxygen in red with arabic numbers used as indices, whereas the roman numbers are showing the oxidation states of Mn ions

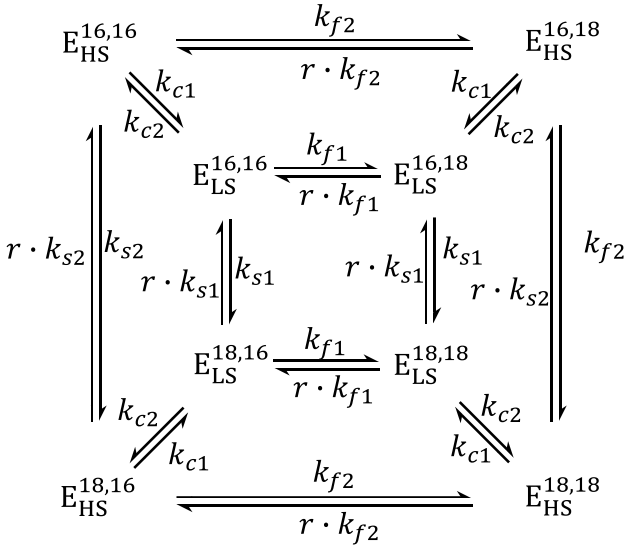

Scheme 1 Substrate-water exchange reactions in a double-conformation model of PSII. Modified after (Huang and Brudvig 2021). E_{HS} and E_{LS} signify the conformations of the HS and LS states of the Mn_4CaO_5 cluster in PSII, while the superscripts ($E^{Ws,Wf}$) indicate the oxygen isotope bound in the binding sites of the slowly (W_S) and fast (W_f) exchanging substrate waters. The exchange rates of W_f and W_S in E_{LS}, E_{HS} are denoted k_{f1}, k_{f2} and k_{s1}, k_{s2}, respectively, while the rates for the E_{HS}/E_{LS} interconversion are noted as k_{c1} and k_{c2}

$$^{34}Y = a\left(1 - e^{-k_f t}\right) + (1-a)\left[b\left(1 - e^{-k_i t}\right) + (1-b)\left(1 - e^{-k_s t}\right)\right]$$

$$^{36}Y = b\left(1 - e^{-k_i t}\right) + (1-b)\left(1 - e^{-k_s t}\right). \quad (3)$$

The k_f rate constant, as before, reflects the fast-exchanging water in both conformations; since the data did not reveal two distinct phases for the fast water exchange, W_f was modeled as a single exchange component. For W_S, however, two components were resolved, of which the faster, k_i, is assigned to the exchange of W_s in HS conformation of the S_2 state (k_{s2} in Scheme 1). For the slower component, k_s, of W_s exchange two possible explanations were given: it could correspond to the W_S exchange in the LS conformation exhibiting the $g = 2.0$ EPR multiline signal (k_{s1} in Scheme 1), or to the rate constant of conformational change, k_{c2} (Scheme 1) of the LS state (E_{LS}) to the HS state (E_{HS}). The coefficient b depends on the equilibrium ratio of the two conformations.

Explicit kinetic modeling of the water exchange has also been done. A numerical solution of the differential equations describing a model with two binding sites and two conformations (Scheme 1) has been applied previously and resulted in exchange rates consistent with those derived by Eq. (3) (de Lichtenberg and Messinger 2020). Recently, Huang and Brudvig (2021) developed the analytical solution for this model, potentially allowing for a more accurate description of the water exchange measurements. However, due to the many terms in the complete analytical solution it is not possible to see the physical meaning and derive unique solutions. Thus, Huang and Brudvig examined some approximations to simplify the expressions. Consistent with our previous work, they conclude that the expressions can be reduced to the form shown in Eq. (3) under the following approximations: (a) the rate of conformational change is much slower than the rates of water exchange; (b) the rate of exchange of W_s is significantly slower than that of W_f, so that W_f exchange is essentially complete before W_S exchange commences; (c) the fast-exchange rate constants in the two conformations are equal. Due to the first approximation, the rates of conformational change are not present in the exponential factors of the simplified equations, and thus the authors concluded, in contrast to de Lichtenberg and Messinger (2020), that the parameter k_{s2} in Eq. (3) cannot correspond to the rate of conformational change between the LS and HS isomers, but only to the rate constant of W_s exchange in the LS conformation. However, this specific approximation is not always satisfied, as seen even in some of the simulations presented in the paper of Huang and Brudvig (2021).

In the following, we revisit the analytic description developed by Huang and Brudvig (2021) and examine other possible simplifications and corrections.

Results and discussion

Non-zero initial $H_2{}^{18}O$ enrichment

The initial conditions (concentrations of each state at time zero) of the system of differential equations are not discussed by Huang and Brudvig (2021). While the coefficients inside of the exponential functions do not depend on the initial conditions, the coefficients in front of the exponentials do. Examining the coefficients given in Ref. Huang and Brudvig (2021), it can be deduced that the authors assumed that at time zero all centers have $H_2{}^{16}O$, and that the equilibrium between the two conformations (dictated by the values of the conformation change rate constants) has already been established at time zero. The first assumption, about all centers holding ^{16}O, is not exactly correct due to the natural abundance of ^{18}O in normal water and due to leakage from the syringe used for injection of labeled water; it has been previously estimated that around 0.7% of the water at time zero has ^{18}O (de Lichtenberg and Messinger 2020). This value is relatively small and does not affect the kinetics of the exchange; however, it may affect the simulations and

fitting of the exchange data at early times. Including this value in the model is straightforward, and the equations describing the yield of single- and double-labeled oxygen for the model with two exchange sites and two conformations are now given by:

$$^{34}\mathrm{Y} \propto \frac{2r}{(1+r)^2}\left[-\frac{1}{r}q^2C_1(t) - \frac{r-1}{2r}qC_2(t) - \frac{r-1}{2r}qC_3(t) + 1\right]$$

$$^{36}\mathrm{Y} \propto \frac{1}{(1+r)^2}\left[q^2C_1(t) - qC_2(t) - qC_3(t) + 1\right]$$

$$C_i(t) = c_i^+ e^{\lambda_i^+ t} + c_i^- e^{\lambda_i^- t}. \tag{4}$$

The equations are identical with the ones in Ref. Huang and Brudvig (2021) (also shown in the Supporting Information), with the addition of the term q that describes the dependence on the initial $H_2{}^{18}O$ enrichment:

$$q = 1 - \frac{1+r}{1+r_0} = 1 - \frac{\alpha_{\mathrm{in}}}{\alpha_{\mathrm{f}}}. \tag{5}$$

Here, r is the equilibrium ratio $\frac{[H_2^{16}O]}{[H_2^{18}O]}$ after the $H_2{}^{18}O$ injection, and r_0 is this ratio before the injection. The pre-exponential coefficients c and the exponential coefficients λ have the same expressions as given in Huang and Brudvig (2021) and in the Supporting Information. The inclusion of this correction to the simulations results in a change that is similar to a shift of the simulated curves to earlier times (see SI Fig. S1a).

HS/LS equilibrium during the substrate exchange

The second assumption that the conformation equilibrium between $S_2{}^{LS}$ and $S_2{}^{HS}$ is already reached at time zero of $H_2{}^{18}O$ incubation is presumably correct for short incubation times when the $H_2{}^{18}O$ injection comes long (10–20 s) after the first flash that advances S_1->S_2, allowing enough time for the conformation equilibration to occur before the injection of labeled water. By contrast, for long incubation times, the injection happens soon after the first flash that generates S_2. Here, the situation is less clear, since low temperature illumination (200 K) of PSII samples in the S_1 state leads predominantly to the formation of $S_2{}^{LS}$, which only upon short warming transforms under suitable conditions into $S_2{}^{HS}$ (Boussac et al. 2018). The rate of this process is presently not well characterized. By contrast, others have concluded on the basis of DFT calculations that the ratio of $S_2{}^{HS}$ to $S_2{}^{LS}$ depends on the distribution of two conformations of the S_1 state (Drosou et al. 2021). Even if that were the case, the equilibrium concentration between the respective conformations would be likely S state dependent and require a presently unknown time to establish. Due to these uncertainties, and the complexity of incorporating this additional equilibration that occurs over variable times into an already highly sophisticated model, we accept the assumption and make no attempt to include it here.

Non-instant injection

In reality, the injection of $H_2{}^{18}O$ into the PSII suspension and the subsequent mixing is not instant. The injection and mixing can be observed using a fluorescent dye (PSII or fluorescein) (Messinger et al. 1995; Nilsson et al. 2014a), and is approximately linear, taking place within around 6 ms. To evaluate the effect of the mixing on the exchange curves, we consider the exchange at a single site. The relative fraction of sites with labeled water, E^{18}, can be described by:

$$\frac{\mathrm{d}E^{18}}{\mathrm{d}t} = k\left(\alpha(t) - E^{18}(t)\right), \tag{6}$$

where k is the apparent rate constant of the exchange, and α is the enrichment of labeled water in the bulk. If α is a constant equal to the final enrichment α_{f}, this has the solution:

$$E^{18}_{\mathrm{instantmixing}}(t) = \alpha_{\mathrm{in}} + (\alpha_{\mathrm{f}} - \alpha_{\mathrm{in}})\left(1 - e^{-kt}\right). \tag{7}$$

This would describe the situation where the injection of labeled water is instantaneous and happens at $t=0$.

Due to the time course for the injection and mixing, the enrichment is initially not constant but increases linearly, starting at $t=0$ at α_{in} until a time $t=t_m$ (which is approximately 6 ms for our experiments), when it reaches α_{f}:

$$\alpha(t) = \begin{cases} \alpha_{\mathrm{in}} + \frac{\alpha_{\mathrm{f}} - \alpha_{\mathrm{in}}}{t_m} t \text{ if } 0 \le t \le t_m \\ \alpha_{\mathrm{f}} \text{ if } t \ge t_m \end{cases} \tag{8}$$

In the two regions, the solution of (6) is now:

$$E^{18}_{\mathrm{linearmixing}}(t) = \begin{cases} \alpha_{\mathrm{in}} + \left(\alpha_{\mathrm{f}} - \alpha_{\mathrm{in}}\right)\frac{\left(e^{-kt} - 1 + kt\right)}{kt_m} \text{ if } 0 \le t \le t_m \\ \alpha_{\mathrm{in}} + \left(\alpha_{\mathrm{f}} - \alpha_{\mathrm{in}}\right)\left(1 - e^{-k(t-t_k)}\right) \text{ if } t \ge t_m \end{cases} \tag{9}$$

Since all points of the water exchange data are measured at times $t \ge t_m = 6$ ms, only the second time region in Eq. (9) is relevant. In this region, the expression for non-instantaneous injection (9) differs from the one for instantaneous injection (7) only by the factor t_k, in a way that one is a time-shifted version of the other, with a time shift given by t_k:

$$E^{18}_{\mathrm{linearmixing}}(t) = E^{18}_{\mathrm{instantmixing}}\left(t - t_k\right). \tag{10}$$

The coefficient t_k depends on the apparent rate constant of water exchange k:

$$t_k = \frac{\ln\left(\frac{e^{kt_m}-1}{kt_m}\right)}{k}. \quad (11)$$

The value of t_k approaches $t_m/2 = 3$ ms for small k, staying close to that value for most of the relevant values of k, only increasing above 3.3 ms for $k > 200$ s^{-1} (see SI Fig. S2 for a plot of t_k as a function of k). At higher values of k, the exchange happens faster than the time resolution of the TR-MIMS experiment, with or without the linear mixing correction. Therefore, we simply use a value of $t_k = 3$ ms and expression (10) to approximate the effect of non-instant injection and mixing. The inclusion of this correction to the simulations results in a shift of the simulated curves to later times (see SI Fig. S1b), which is in opposite direction of the correction for non-zero initial $H_2{}^{18}O$ enrichment.

Water exchange in the S_3 state affecting the S_2 state exchange measurements

In the TR-MIMS experiments, when water exchange in the S_2 state is measured, the PSII sample is first brought into the S_2 state by one excitation light flash, then labeled water is injected into the sample, and after a varying incubation time two more light flashes are given to drive the O_2 evolution reaction. The first of the two extra flashes brings the sample to the S_3 state, where it spends a very short time, usually 10 ms, before the next flash that drives the $S_3 \rightarrow S_0 + O_2$ step. The time is short, in order to minimize the effect on the observed isotope ratios due to exchange in the S_3 state, but must remain long enough to allow re-opening of the acceptor side and, thereby, advancement of a significant fraction to S_0 coupled to O_2 production. We note that for short $H_2{}^{18}O$ incubation times in the S_2 state, and for relatively fast S_3 exchange kinetics, the effect might be significant and we thus recently started to account for it [see SI of de Lichtenberg et al. (2021)]. Knowing the water exchange rates in the S_3 state, it is possible to account for the 10 ms S_3 state exchange on the simulated S_2 state exchange kinetics by doing an extra simulation for each time point, where one takes the final concentrations of the components from the S_2 exchange simulation and uses them as initial concentrations for a 10 ms exchange using the S_3 exchange rate constants [see SI of de Lichtenberg et al. (2021)]. This assumes that the fast- and slow-exchanging sites observed in S_2 correspond to the fast- and slow-exchanging sites in S_3. This correction results in the apparent shift of the simulated curves to earlier times (see SI Fig. S1c), opposite to the effect of the correction for non-instant mixing. This extra exchange in the S_3 state is ignored in the model of Huang and Brudvig (2021).

Applying all three corrections to the simulation has their effects mostly canceling each other (see SI Fig. S1d), and thus not considering them should not affect the interpretation of the data in a major way, at least in most cases when the exchange in S_3 is relatively slow. Nevertheless, in the rest of this work, all simulations are performed applying all three corrections.

Interpretation of the water exchange data with the analytical solution of the two-site double-conformation model

The analytical solution of the two-site double-conformation model (Scheme 1) is a linear combination of a total of 8 exponential terms (Eq. 4) (Huang and Brudvig 2021). The arguments of the exponential functions are the $H_2{}^{18}O$ incubation time multiplied by the eigenvalues of the rate constants matrix (one of them is zero, yielding a constant term). To make physical sense of the results, Huang and Brudvig applied two approximations that simplify the expressions: firstly, the rates of conversion between the two conformations (with rate constants k_{c1} and k_{c2}) are both significantly slower than all other rates, and secondly, the fast exchange (with apparent rate constants k^*_{f1} and k^*_{f2}) is significantly faster than the slow exchange (k^*_{s1} and k^*_{s2}). The authors then arrive at simple approximate expressions that show that the yield of double-labeled O_2 (^{36}Y) is a sum of two exponentials with rate constants equal to the two slow exchange constants, k^*_{s1} and k^*_{s2}. Both the constants come from the third eigenvalue pair, $\lambda_3^{+/-}$ in Eq. (4) [Eq. 30 in Huang and Brudvig (2021)]; due to the assumption that $k^*_f \gg k^*_s$, the terms containing $\lambda_1^{+/-}$ and $\lambda_2^{+/-}$ cancel each other. The yield of single-labeled O_2 (^{34}Y) adds two more exponentials with constants equal to the fast-exchange constants. The rate constants of interconversion between the two conformations appear only in the pre-exponential coefficients, but not as parameters of the exponential functions in this simplification. However, while the approximation that $k^*_f \gg k^*_s$ is presumably valid under most circumstances, the assumption that $k^*_s \gg k_c$ may not hold in all cases; for example, in the simulations of the Sr^{2+}-PSII data at pH 8.3 presented in Table 2 of Ref. Huang and Brudvig (2021) the conformation change rate constants k_c are significantly larger than one of the rate constant of the slow exchange k^*_s.

A different simplification of the equations and a different interpretation of the experimental data is possible, which is not discussed by Huang and Brudvig (2021). In this approximation, only one of the slow exchange rates (k^*_{s1} or k^*_{s2}) needs to be significantly faster than only one of the rate constants of conformation change (k_{c1} or k_{c2}). This would lead to the other conformation change rate appearing in the approximate expressions for ^{34}Y and ^{36}Y. We first note that the (exact)

expression for the third pair of eigenvalues can be rewritten as:

$$\lambda_3^{+,-} = \frac{1}{2}\left[-\left(k_{s1}^* + k_{s2}^* + k_{c1} + k_{c2}\right) \pm \sqrt{\left(-k_{s1}^* + k_{s2}^* + k_{c1} - k_{c2}\right)^2 + 4k_{c1}k_{c2}}\right]. \quad (12)$$

With the relaxed approximation requirements, we can neglect only the term $4k_{c1}k_{c2}$ in the above expression, which allows us to cancel the square and square root, yielding the following two approximate expressions for the eigenvalues:

$$\lambda_3^+ \approx -\left(k_{s1}^* + k_{c2}\right),\ \lambda_3^- \approx -\left(k_{s2}^* + k_{c1}\right). \quad (13)$$

If both k_{s1}^* and k_{s2}^* are significantly larger than k_{c1} and k_{c2} we still get, as in Huang and Brudvig (2021):

$$\lambda_3^+ \approx -k_{s1}^*,\ \lambda_3^- \approx -k_{s2}^*. \quad (14)$$

However, in the case when e.g., $k_{s1}^* \ll k_{c2}$, we get instead:

$$\lambda_3^+ \approx -k_{c2},\ \lambda_3^- \approx -k_{s2}^*. \quad (15)$$

This would mean that the two phases observed in the yield of double-labeled O_2 (^{36}Y) would not reflect the exchange of W_S in the two conformations, but instead the rate of exchange in E_{HS} and the conversion of E_{LS} to E_{HS} (Scheme 1). This corresponds to the second interpretation obtained by de Lichtenberg and Messinger (2020) employing Eq. (3).

For example, using the values from the first simulation for the Sr-PSII sample at pH 8.3 presented in Ref. Huang and Brudvig (2021) and shown in Table 1, the exact values of the two eigenvalues (Eq. 12, not approximated) are $\lambda_3^+ = -11.96\ s^{-1}$ and $\lambda_3^- = -54.64\ s^{-1}$. It is only these two kinetic phases that can be seen in the ^{36}Y trace, although they are not clearly visibly separated, as the two values are not sufficiently different (Fig. 3C, blue trace). The $\lambda_3^- = -54.64\ s^{-1}$ component is associated with the slow water exchange in E_{HS}, $k_{s2}^* = 50\ s^{-1}$. The $\lambda_3^+ = -11.96\ s^{-1}$ component, however, matches the approximations given (Eq. 15) very well ($\lambda_3^+ = -11.96\ s^{-1} \approx -k_{c2} = -12\ s^{-1}$) and does not match the approximations (Eq. 14) given in Ref. Huang and Brudvig (2021) ($-11.96\ s^{-1} \neq -k_{s1}^* = -1\ s^{-1}$), and thus reflects the conversion of E_{LS} to E_{HS} and not the exchange in E_{LS}.

In other simulations, the kinetic components observed in ^{36}Y do correspond to the slow water exchange in the two conformations, k_{s1}^* and k_{s2}^*, see the Ca^{2+}-PSII, pH 8.6 and Sr^{2+}-PSII, pH 6.0 simulations taken from Ref. Huang and Brudvig (2021) in Table 1 and Fig. 3A and B, black traces (mostly covered). However, these are not the only possible simulations that give the same fit quality. Depending on the values at which we choose to fix k_{s1}^*, we can obtain simulations in which the simulated ^{34}Y and ^{36}Y curves are practically identical, but for which the slowest observed kinetic component (with a rate of around $1\ s^{-1}$ for both samples) corresponds not to k_{s1}^* but to k_{c2} (blue traces in Fig. 3A and B). The two kinetic components in ^{36}Y are especially well separated in the Sr^{2+}-PSII, pH 6.0 simulations (Figs. 1B, S3), and correspond to the eigenvalues $\lambda_3^+ = -1.31\ s^{-1} \approx -k_{c2}$ and $\lambda_3^- = -27\ s^{-1} \approx -k_{s2}^*$ for the blue trace in Fig. 3B. Two interpretations of the exchange data in the Sr^{2+}-PSII sample at pH 8.3 are also possible, see for example the last simulation in Table 1 and the black traces in Fig. 3C, where the two kinetic components in ^{36}Y correspond to k_{s1}^* and k_{s2}^*. We, therefore, conclude, in line with our previous work (de Lichtenberg and Messinger 2020), that it is not possible to tell from the simulations if the slowest observed kinetic component in the TR-MIMS traces corresponds to the slow

Table 1 Summary of the rate constants obtained from the substrate-water exchange experiments (de Lichtenberg and Messinger 2020) using the analytical solution of the extended form (see above) of the double-conformation model presented by Huang and Brudvig (2021)

Sample	Model	k_{f1}^*	k_{f2}^*	k_{s1}^*	k_{s2}^*	k_{c1}	k_{c2}	k_{c2}/k_{c1}	Chi^2
Ca^{2+}-PSII, pH 8.6	Ref. Huang and Brudvig (2021)	94 (fixed)	73 ± 14	1.1 (fixed)	11.7 ± 1.3	0.084 ± 0.13	0.62 ± 0.63	7.5 ± 1.5	0.11
	This work	94 (fixed)	73 ± 20	0.01 (fixed)	11 ± 1	0.13 ± 0.1	1.5 ± 0.7	12 ± 4	0.11
Sr^{2+}-PSII, pH 6.0	Ref. Huang and Brudvig (2021)	120 (fixed)	75 ± 21	1.0 (fixed)	28.6 ± 13.5	0.30 ± 0.30	0.32 ± 0.23	1.0 ± 0.2	0.14
	This work	120 (fixed)	75 (fixed)	0.01 (fixed)	26 ± 7	1.1 ± 0.4	1.3 ± 0.2	1.2 ± 0.2	0.14
Sr^{2+}-PSII, pH 8.3	Ref. Huang and Brudvig (2021)	120 (fixed)	65 ± 9	1.0 (fixed)	50 ± 10	3.6 ± 2.9	12 ± 6	3.4 ± 1.8	0.18
	This work	120 (fixed)	65 (fixed)	11 ± 3	57 ± 14	0.6 ± 0.3	1.0 (fixed)	1.6 ± 1.5	0.18

k^* denotes apparent rate constants. The first subscript of k^* denotes the kind of rate constant (fast or slowly exchanging), and k_c is the conformational change rate constant. The second subscript of k denotes the conformation, see Scheme 1. All rate constants are in unit s^{-1}. The errors of the fit parameters are estimated from the bootstrapping distributions (shown in SI Figs. S4–S6 for the models in this work). The simulated curves are shown in Fig. 3

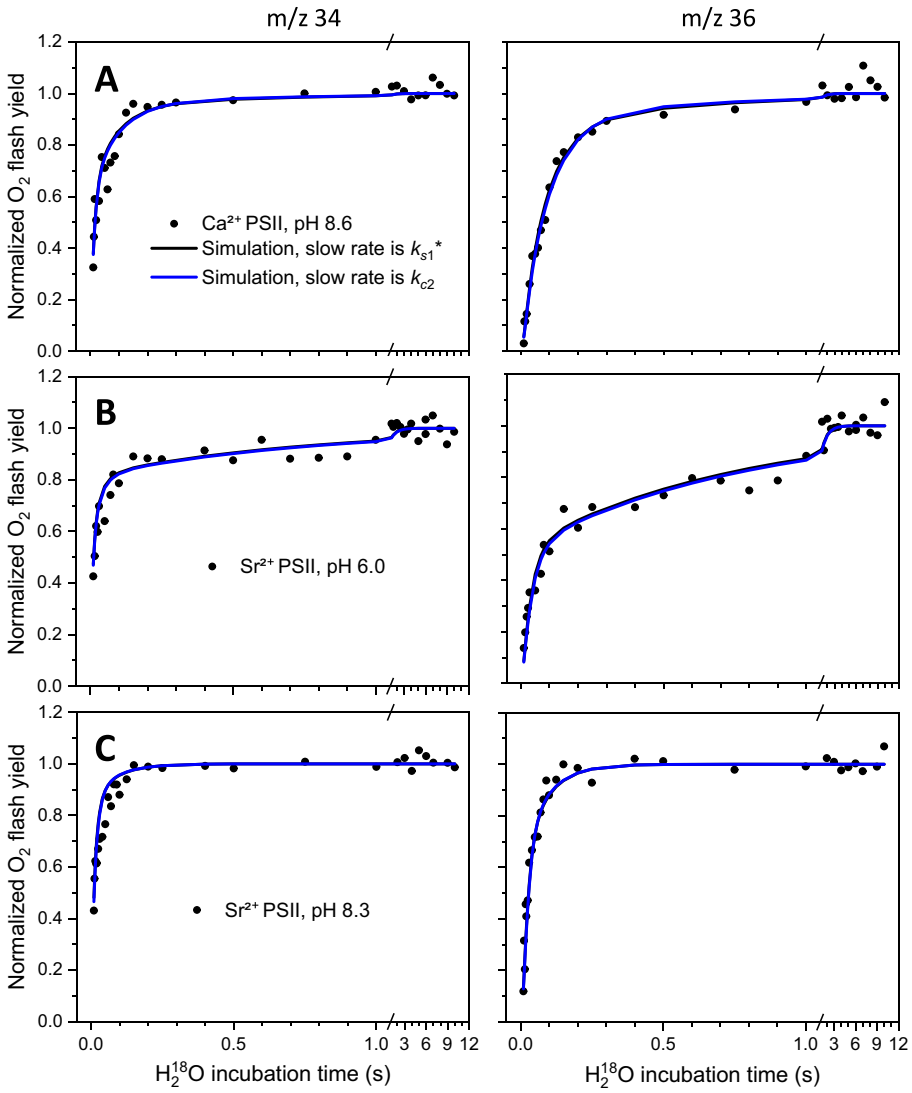

Fig. 3 Substrate-water exchange data in two-conformation systems in the S_2 state taken from Ref. de Lichtenberg and Messinger (2020) and simulated using our extended form of the double-conformation model (Scheme 1) presented in Huang and Brudvig (2021). The single-labeled O_2 yield (^{34}Y) is shown on the left, and the double-labeled O_2 yield (^{36}Y) is shown on the right. Black dots show individual experimental data points. The black and the blue curves (mostly overlapping) show simulations using rate constants given in Table 1, for the cases when the slowest kinetic component corresponds either to the slow water exchange in E_{LS} (k_{s1}^*, black) or to the rate constant for the conversion of E_{LS} to E_{HS} (k_{c2}, blue). The intermediate kinetic component is explained in all simulations by the slow water exchange in E_{HS}. Corrections for initial enrichment ($\alpha_{in}=0.7\%$), non-instant injection ($t_k=3$ ms), and exchange in S_3 (with additional 10 ms exchange using rate constants $k_f^* = 19.5, k_s^* = 0.25\ s^{-1}$) are applied for all simulations. **A** Ca^{2+}-PSII, pH 8.6; **B** Sr^{2+}-PSII, pH 6.0; **C** Sr^{2+}-PSII, pH 8.3

water exchange in the LS state or to the rate of conversion of E_{LS} to E_{HS}.

Discussion

The present re-evaluation of the analytical solution obtained by Huang and Brudvig (2021) for water exchange in the high spin (E_{HS}) and low spin (E_{LS}) conformations of the S_2 state of photosystem II shows that the simplifications required for interpreting the results lead to the same two possibilities as proposed previously by de Lichtenberg and Messinger (2020): firstly (solution 1), the two kinetic phases in the ^{36}Y data correspond to the slow exchange constants (k_{s1} and k_{s2}) in the two conformations; this requires that the conformational equilibrium is much slower than the slow exchange rates in the two conformations. Secondly (solution 2), the faster of the slow exchange rates corresponds to the slow exchange in the S_2^{HS} state (E_{HS}) that promotes W_s exchange, while the slower ^{36}Y rise reflects the rate of conversion of E_{LS} to E_{HS} that promotes W_s exchange [see also de Lichtenberg and Messinger (2020)]. A molecular interpretation of this important result with regard to the binding site of W_s in the Mn_4CaO_5 cluster is complicated by the fact that the structure of E_{HS} remains controversial due to the absence of reliable x-ray diffraction or cryoEM data of PSII in the S_2^{HS} state(s) (Fig. 2A–C).

Previous substrate-water exchange measurements, advanced EPR experiments with ^{17}O labeling, and computational studies have indicated O5 as the slow-exchanging substrate (Messinger 2004; Siegbahn 2009, 2013; Rapatskiy et al. 2012; Cox and Messinger 2013). In the well-established low spin (multiline) conformation of the S_2 state (E_{LS} in Scheme 1), O5 is bound as a μ_3-oxo bridge between Mn4, Mn3, and Ca, with both Mn ions being in the formal oxidation state IV (Fig. 1). Thus, O5 is expected

to be rather exchange inert in the E_{LS} conformation of the S_2 state (Hillier and Wydrzynski 2001, 2008; Tagore et al. 2006, 2007), consistent with solution 2 in which one of the states is exchange inert and the slower phase of the ^{36}Y rise is reflecting the rate of E_{LS} to E_{HS} conversion. Siegbahn calculated an exchange mechanism for O5 in the S_2^{LS} state (E_{LS} in Scheme 1) that involves water binding to Mn1 and proton transfer to O5 coupled with stepwise electron transfer from Mn1 via Mn3 to Mn4 (Siegbahn 2013). In this sequence, O5 finally ends up being fully protonated and ligated as terminal ligand at Mn4(III), where it then can exchange with water surrounding the cluster ('cavity' water). The calculated rate-limiting barrier for this transition is surprisingly close in energy to the experimentally determined value (Hillier and Wydrzynski 2000; Siegbahn 2013). However, it may also be possible that a modified solution 1 is at play in which the two rate constants k^*_{s1} and k^*_{s2} reflect the exchange in E_{LS} and E_{HS}, respectively, and where the exchange rates are limited by the different activation barriers for water binding to Mn1, thus a structural change not explicitly included in Scheme 1 [see also discussion in de Lichtenberg and Messinger (2020)].

The second conformation (E_{HS} in Scheme 1), in which O5 exchanges faster, was associated with the high spin state on the basis of its prominence at high pH and its sensitivity to ammonia addition as well as Ca/Sr exchange (de Lichtenberg and Messinger 2020), properties of the high spin state established earlier by Boussac and coworkers (Boussac et al. 2018). Nevertheless, while the correlation appears convincing, it cannot be fully excluded that the state promoting W_s exchange is not identical to the high spin state.

Of the three dominant proposals for the high spin S_2 state (S_2^{HS}), one involves a closed cubane conformation Fig. 2A) (Pantazis et al. 2012; Isobe et al. 2012; Bovi et al. 2013). In this conformation, O5 is bound as μ_3-oxo bridge between Mn1, Mn3, and Ca, and both ligating Mn ions are in oxidation state IV. Thus, it is not obvious as to why O5 would exchange more rapidly in this conformation. By contrast, such a structure would be more likely to promote a faster W2 or O4 exchange, which are alternative assignments for W_s in the literature [for discussion, see de Lichtenberg and Messinger (2020), Huang and Brudvig (2021)]. However, while several theoretical studies consistently identify the high spin state with a closed cubane structure (Pantazis et al. 2012; Isobe et al. 2012; Bovi et al. 2013), several experimental approaches targeted to elucidating the high spin structure found no evidence for this conformation (Chatterjee et al. 2019; Pushkar et al. 2019).

In the second proposed structure of the S_2^{HS} conformation (Fig. 2B), early water binding to the Mn1 site is suggested, mostly for alkaline conditions (Pushkar et al. 2019; de Lichtenberg and Messinger 2020). Such a state is similar in structure to one of the intermediates of Siegbahn's proposed O5 exchange pathway (Siegbahn 2013; de Lichtenberg and Messinger 2020). Thus, it may be plausible that in this state O5 would exchange more rapidly, assuming that reaching the water(hydroxide)-bound state would be rate limiting in E_{LS} at neutral pH [see discussion in de Lichtenberg and Messinger (2020)].

In the third suggested S_2^{HS} state structure (Fig. 2C), mostly proposed for neutral or slightly acidic conditions, a proton from W1 is shifted to the O4-bidge (Corry and O'Malley 2019). This proton shift would likely promote O5 exchange by either (i) making deprotonation of water to hydroxide easier during binding to Mn1 via providing a suitable base ($W1 = OH^-$) and/or (ii) enabling O5 protonation via the trans effect of OH^- in the W1 position. Thus, also this structural proposal is consistent with the S_2^{HS} (E_{HS}) state being faster exchanging than the S_2^{LS} (E_{LS}) state.

Vinyard et al. (2015) and Vinyard and Brudvig (2017) proposed an exchange model for substrate water in which they aimed to reconcile their expectation that O5 is not exchangeable in the S_2 and S_3 states with experimental evidence that O5 can exchange in the S_1 state with rates consistent with those of W_s (Rapatskiy et al. 2012). In their proposal, W2 bound to Mn4(III) is, in the S_0 and S_1 states, in exchange equilibrium with both the bulk water and O5; thus, it exchanges at an unresolved fast rate (together with W3) with bulk water, and additionally with a slow rate with O5. In the S_2 and S_3 states, the slow exchange of W2 with O5 is proposed to be blocked because O5 then binds between two Mn(IV) ions. Instead, it is proposed that the accumulation of a positive charge during the $S_1 \rightarrow S_2$ transition dramatically slows the exchange of the Ca-bound W3. In this explanation, W_s binding would be consistent with the acceleration of its exchange upon Ca/Sr substitution, but in conflict with known exchange rates for Ca-bound water (Helm and Merbach 2005; Hillier and Wydrzynski 2008). On that basis, Vinyard and Brudvig propose that O–O bond formation occurs between W2 and W3 via nucleophilic attack. While interesting, this proposal is inconsistent with available substrate-water exchange data and kinetic considerations: since the two proposed substrates W2 and W3 exchange rapidly with the essentially endless pool of bulk water in the S_1 and S_2 states, and W2 equilibration with O5 is more than 100-fold slower than the unresolved rapid exchange with bulk water, no slow phase but instead an essentially instantaneous complete exchange of 'W_s' (W2) would be observable in both the ^{34}Y and ^{36}Y data for the S_0 and S_1 states, in stark contrast to experimental observations that clearly reveal the slow exchange phase.

Huang and Brudvig (2021) concluded, on the basis of their analysis and by favoring the closed cube model for S_2^{HS} (E_{HS}), that W1 and/or W2 may be substrate waters. In contrast the team's earlier publications (Vinyard et al. 2015; Vinyard and Brudvig 2017), they excluded that Ca-bound W3 and W4 can be a substrate due to their weak association

with Ca. However, no specific suggestion regarding a mechanism was made.

In 2013, Vinyard and Dismukes published a molecular explanation for the substrate exchange rates (Vinyard et al. 2013). While several features are similar to our earlier proposal (Messinger 2004), such as employing a closed cube conformation and assigning W_f to W2 and W_s to O5, this interpretation is based on the low-oxidation state paradigm in which the S_1 state has the oxidation states Mn_4(III,III,III,III). Additionally, special emphasis was given to explain the S_i state dependence of the exchange rates by changes in the Jahn–Teller axes of the Mn(III) ions connected to O5. The main argument against this mechanism is the convincing evidence for the high-oxidation state paradigm (Yachandra et al. 1996; Haumann et al. 2005; Kulik et al. 2007; Siegbahn 2009; Cox et al. 2014; Krewald et al. 2015; Cheah et al. 2020) and the experimental verification that the S_3 state contains an extra oxygen bridge (Suga et al. 2017; Kern et al. 2018), see however Wang et al. (2021).

The analysis obtained here is fully consistent with the picture derived by us over the years by combining substrate-water exchange results with structural information from advanced EPR and snapshot crystallography at XFELs (Messinger 2004; Rapatskiy et al. 2012; Cox and Messinger 2013; Navarro et al. 2013; Nilsson et al. 2014b; Kern et al. 2018; de Lichtenberg and Messinger 2020; Ibrahim et al. 2020; de Lichtenberg et al. 2021; Hussein et al. 2021; Bhowmick et al. 2023). In this model, for substrate-water binding and O–O bond formation (Fig. 4), O5 is the slowly exchanging substrate in all S states, while W3 bound as terminal ligand to Ca may be identified as the fast-exchanging substrate in the S_0, S_1, and S_2 states [although in rapid exchange equilibrium with all other water molecules in the inner cavity (de Lichtenberg et al. 2021)]. In these early S states, W_f exchange is limited by isotopic equilibration through barriers in the channels connecting the bulk and the Mn_4CaO_5 cluster (Vassiliev et al. 2012; de Lichtenberg et al. 2021), while during the $S_2 \rightarrow S_3$ transition W_f moves into the O_X/O6 position that bridges Ca and Mn1. The binding of W_f to Mn in the S_3 state is consistent with its slower exchange in S_3 compared to the earlier S states. Since in the major S_3 state conformation all Mn ions of the cluster are in the Mn(IV) state (Haumann et al. 2005; Cox et al. 2014; Kern et al. 2018; Schuth et al. 2018) and thus are exchange inert, its rate of exchange may be limited by the back donation of one electron from Y_Z (Siegbahn 2013; Nilsson et al. 2014b; de Lichtenberg et al. 2021), i.e., by the formation of the $S_2'Y_Z^{ox}$ state. Nevertheless, also S_3 minority species are proposed in which Mn(III) ions may be formed by partial oxygen ligand oxidation, such as oxyl radical or peroxide formation (Isobe et al. 2019; Corry and O'Malley 2021). While peroxide formation between the substrates is expected to fully block exchange, oxyl radical formation may initiate water exchange under certain conditions.

In principle, also two kinetic phases for W_f exchange may be expected and are indeed included in Scheme 1.

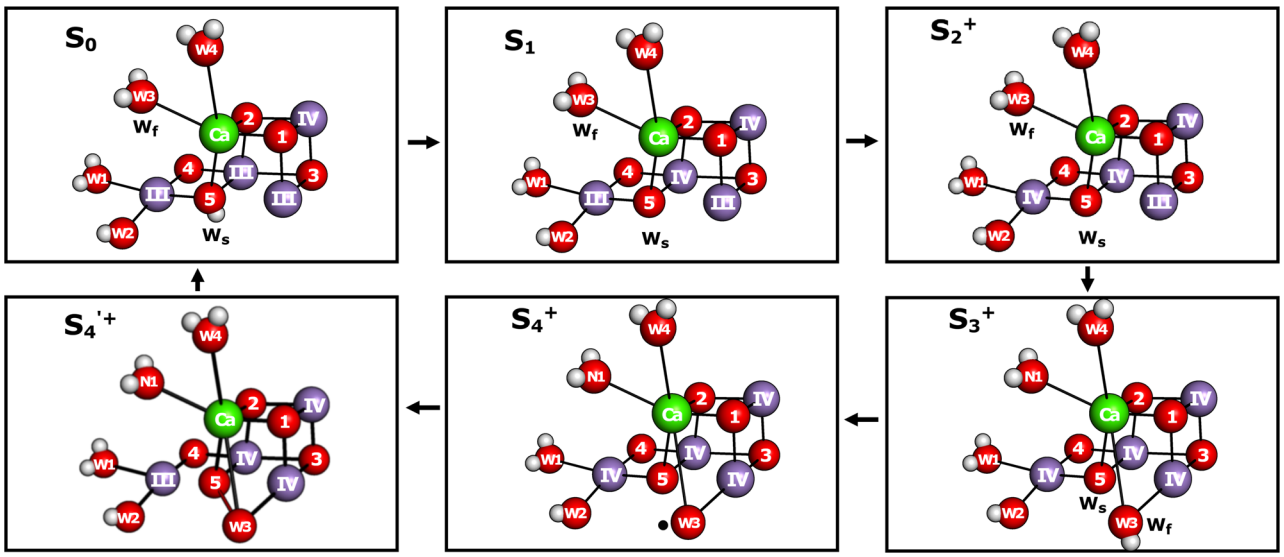

Fig. 4 A schematic presentation of the OEC conformations of the S states during the Kok cycle, based on previous spectroscopic, structural, and DFT results, see Text. The oxygens proposed to be the fast and slowly exchanging substrate waters are denoted as W_f and W_s, respectively, for states their exchange rates have been measured. N1 signifies a new water molecule that replaces W3 at Ca during the $S_2 \rightarrow S_3$ transition. A second water binding event during the reconstruction of the cluster after O_2 release in the $S_4 \rightarrow S_0$ transition, as well as proton and O_2 release are not indicated for simplicity of presentation. Manganese atoms are shown in magenta, calcium in green, and oxygen in red with Arabic numbers. Roman numbers indicate the oxidation states of manganese ions

However, the apparent rates, k^*_{f1} and k^*_{f2}, are within a factor of 2 (Table 1), consistent with the experimental observation that under most circumstances only one fast phase can be observed. The inability to resolve two fast rates is consistent with the above picture that W_f exchange in the S_2 state is limited by equilibration of all 'cavity' waters around the Mn_4CaO_5 cluster with bulk water (de Lichtenberg et al. 2021), which effectively prevents the observation of possible chemical differences in W_f binding between E_{LS} and E_{HS}.

In our model, exchange of W_s (O5) in S_3 state is dependent on Mn(III) formation, e.g., via Y_Z back donation, but slower than W_f exchange because additional significant barriers are involved for its exchange.

Conclusion

The present extension of the analytical analysis of the two-state two-conformation model for the S_2 state (Scheme 1) and its interpretation in the context of literature data reconciles the expected non-exchangeability of O5 when bound between Mn(IV) ions (Tagore et al. 2006, 2007) with the experimental and theoretical assignment of O5 as the slowly exchanging substrate water in all S states (Messinger 2004; Siegbahn 2009; Rapatskiy et al. 2012; Cox and Messinger 2013), and excludes the alternative substrate water assignments in the literature (Vinyard et al. 2013, 2015; Vinyard and Brudvig 2017).

Supplementary Information The online version contains supplementary material available at https://doi.org/10.1007/s11120-024-01084-8.

Acknowledgements This work was supported by the Swedish Science Foundation (Vetenskapsrådet; Grant Nr.: 2020-03809).

Author contributions Johannes Messinger designed, supervised and provided funding for the study. Petko Chernev performed calculations and wrote the first draft of the manuscript. Johannes Messinger and A. Orkun Aydin revised the manuscript. Petko Chernev and A. Orkun Aydin prepared the figures.

Funding Open access funding provided by Uppsala University.

Data availability Original data will be provided upon request.

Declarations

Competing interests JM is Editor-in Chief of *Photosynthesis Research* but was not involved in the evaluation of this manuscript. PC and AOA declare they have no financial or non-financial interests.

References

Bhowmick A, Hussein R, Bogacz I, Simon PS, Ibrahim M, Chatterjee R, Doyle MD, Cheah MH, Fransson T, Chernev P, Kim I-S, Makita H, Dasgupta M, Kaminsky CJ, Zhang M, Gätcke J, Haupt S, Nangca II, Keable SM, Aydin AO, Tono K, Owada S, Gee LB, Fuller FD, Batyuk A, Alonso-Mori R, Holton JM, Paley DW, Moriarty NW, Mamedov F, Adams PD, Brewster AS, Dobbek H, Sauter NK, Bergmann U, Zouni A, Messinger J, Kern J, Yano J, Yachandra VK (2023) Structural evidence for intermediates during O_2 formation in photosystem II. Nature 617:629–636. https://doi.org/10.1038/s41586-023-06038-z

Boussac A, Ugur I, Marion A, Sugiura M, Kaila VRI, Rutherford AW (2018) The low spin–high spin equilibrium in the S_2-state of the water oxidizing enzyme. Biochim Biophys Acta 1859(5):342–356. https://doi.org/10.1016/j.bbabio.2018.02.010

Bovi D, Narzi D, Guidoni L (2013) The S_2 state of the oxygen-evolving complex of photosystem II explored by QM/MM dynamics: spin surfaces and metastable states suggest a reaction path towards the S_3 state. Angew Chem Int Ed 52(45):11744–11749. https://doi.org/10.1002/anie.201306667

Chatterjee R, Lassalle L, Gul S, Fuller FD, Young ID, Ibrahim M, de Lichtenberg C, Cheah MH, Zouni A, Messinger J, Yachandra VK, Kern J, Yano J (2019) Structural isomers of the S_2 state in photosystem II: do they exist at room temperature and are they important for function? Physiol Plant 166(1):60–72. https://doi.org/10.1111/ppl.12947

Cheah MH, Zhang M, Shevela D, Mamedov F, Zouni A, Messinger J (2020) Assessment of the manganese cluster's oxidation state via photoactivation of photosystem II microcrystals. Proc Natl Acad Sci USA 117(1):141–145. https://doi.org/10.1073/pnas.1915879117

Corry TA, O'Malley PJ (2019) Proton isomers rationalize the high- and low-spin forms of the S_2 state intermediate in the water-oxidizing reaction of photosystem II. J Phys Chem Lett 10(17):5226–5230. https://doi.org/10.1021/acs.jpclett.9b01372

Corry TA, O'Malley PJ (2021) S_3 state models of nature's water oxidizing complex: analysis of bonding and magnetic exchange pathways, assessment of experimental electron paramagnetic resonance data, and implications for the water oxidation mechanism. J Phys Chem B 125(36):10097–10107. https://doi.org/10.1021/acs.jpcb.1c04459

Cox N, Messinger J (2013) Reflections on substrate water and dioxygen formation. Biochim Biophys Acta 1827:1020–1030. https://doi.org/10.1016/j.bbabio.2013.01.013

Cox N, Retegan M, Neese F, Pantazis DA, Boussac A, Lubitz W (2014) Electronic structure of the oxygen-evolving complex in photosystem II prior to O-O bond formation. Science 345(6198):804–808. https://doi.org/10.1126/science.1254910

Dau H, Limberg C, Reier T, Risch M, Roggan S, Strasser P (2010) The mechanism of water oxidation: from electrolysis via homogeneous to biological catalysis. ChemCatChem 2(7):724–761. https://doi.org/10.1002/cctc.201000126

de Lichtenberg C, Messinger J (2020) Substrate water exchange in the S_2 state of photosystem II is dependent on the conformation of the Mn_4Ca cluster. Phys Chem Chem Phys 22(23):12894–12908. https://doi.org/10.1039/D0CP01380C

de Lichtenberg C, Kim CJ, Chernev P, Debus RJ, Messinger J (2021) The exchange of the fast substrate water in the S_2 state of photosystem II is limited by diffusion of bulk water through channels—implications for the water oxidation mechanism. Chem Sci 12(38):12763–12775. https://doi.org/10.1039/d1sc02265b

Dismukes GC, Siderer Y (1981) Intermediates of a polynuclear manganese cluster involved in photosynthetic oxidation of water. Proc Natl Acad Sci USA 78(1):274–278. https://doi.org/10.1073/pnas.78.1.274

Drosou M, Zahariou G, Pantazis DA (2021) Orientational Jahn-Teller isomerism in the dark-stable state of Nature's water oxidase. Angew Chem Int Ed 60(24):13493–13499. https://doi.org/10.1002/anie.202103425

Greife P, Schönborn M, Capone M, Assunção R, Narzi D, Guidoni L, Dau H (2023) The electron–proton bottleneck of photosynthetic oxygen evolution. Nature 617:623–628. https://doi.org/10.1038/s41586-023-06008-5

Haumann M, Müller C, Liebisch P, Iuzzolino L, Dittmer J, Grabolle M, Neisius T, Meyer-Klaucke W, Dau H (2005) Structural and oxidation state changes of the photosystem II manganese complex in four transitions of the water oxidation cycle ($S_0 \rightarrow S_1$, $S_1 \rightarrow S_2$, $S_2 \rightarrow S_3$, and S_3, $S_4 \rightarrow S_0$) characterized by X-ray absorption spectroscopy at 20 K and room temperature. Biochemistry 44(6):1894–1908. https://doi.org/10.1021/bi048697e

Helm L, Merbach AE (2005) Inorganic and bioinorganic solvent exchange mechanisms. Chem Rev 105(6):1923–1959. https://doi.org/10.1021/cr030726o

Hillier W, Wydrzynski T (2000) The affinities for the two substrate water binding sites in the O_2 evolving complex of photosystem II vary independently during S-state turnover. Biochemistry 39(15):4399–4405. https://doi.org/10.1021/bi992318d

Hillier W, Wydrzynski T (2001) Oxygen ligand exchange at metal sites: implications for the O_2 evolving mechanism of photosystem II. Biochim Biophys Acta 1503(1–2):197–209. https://doi.org/10.1016/S0005-2728(00)00225-5

Hillier W, Wydrzynski T (2008) ^{18}O-Water exchange in photosystem II: substrate binding and intermediates of the water splitting cycle. Coord Chem Rev 252:306–317. https://doi.org/10.1016/j.ccr.2007.09.004

Hillier W, Messinger J, Wydrzynski T (1998) Kinetic determination of the fast exchanging substrate water molecule in the S_3 state of photosystem II. Biochemistry 37(48):16908–16914. https://doi.org/10.1021/bi980756z

Huang H-L, Brudvig GW (2021) Kinetic modeling of substrate-water exchange in photosystem II. BBA Adv 1:100014. https://doi.org/10.1016/j.bbadva.2021.100014

Hussein R, Ibrahim M, Bhowmick A, Simon PS, Chatterjee R, Lassalle L, Doyle M, Bogacz I, Kim IS, Cheah MH, Gul S, de Lichtenberg C, Chernev P, Pham CC, Young ID, Carbajo S, Fuller FD, Alonso-Mori R, Batyuk A, Sutherlin KD, Brewster AS, Bolotovsky R, Mendez D, Holton JM, Moriarty NW, Adams PD, Bergmann U, Sauter NK, Dobbek H, Messinger J, Zouni A, Kern J, Yachandra VK, Yano J (2021) Structural dynamics in the water and proton channels of photosystem II during the S_2 to S_3 transition. Nat Commun. https://doi.org/10.1038/s41467-021-26781-z

Ibrahim M, Fransson T, Chatterjee R, Cheah MH, Hussein R, Lassalle L, Sutherlin KD, Young ID, Fuller FD, Gul S, Kim IS, Simon PS, de Lichtenberg C, Chernev P, Bogacz I, Pham CC, Orville AM, Saichek N, Northen T, Batyuk A, Carbajo S, Alonso-Mori R, Tono K, Owada S, Bhowmick A, Bolotovsky R, Mendez D, Moriarty NW, Holton JM, Dobbek H, Brewster AS, Adams PD, Sauter NK, Bergmann U, Zouni A, Messinger J, Kern J, Yachandra VK, Yano J (2020) Untangling the sequence of events during the $S_2 \rightarrow S_3$ transition in photosystem II and implications for the water oxidation mechanism. Proc Natl Acad Sci USA 117(23):12624–12635. https://doi.org/10.1073/pnas.2000529117

Isobe H, Shoji M, Yamanaka S, Umena Y, Kawakami K, Kamiya N, Shen JR, Yamaguchi K (2012) Theoretical illumination of water-inserted structures of the $CaMn_4O_5$ cluster in the S_2 and S_3 states of oxygen-evolving complex of photosystem II: full geometry optimizations by B3LYP hybrid density functional. Dalton Trans 41(44):13727–13740. https://doi.org/10.1039/C2dt31420g

Isobe H, Shoji M, Suzuki T, Shen JR, Yamaguchi K (2019) Spin, valence, and structural isomerism in the S_3 state of the oxygen-evolving complex of photosystem II as a manifestation of multimetallic cooperativity. J Chem Theory Comput 15(4):2375–2391. https://doi.org/10.1021/acs.jctc.8b01055

Junge W (2019) Oxygenic photosynthesis: history, status and perspective. Q Rev Biophys. https://doi.org/10.1017/S0033583518000112

Kern J, Chatterjee R, Young ID, Fuller FD, Lassalle L, Ibrahim M, Gul S, Fransson T, Brewster AS, Alonso-Mori R, Hussein R, Zhang M, Douthit L, de Lichtenberg C, Cheah MH, Shevela D, Wersig J, Seuffert I, Sokaras D, Pastor E, Weninger C, Kroll T, Sierra RG, Aller P, Butryn A, Orville AM, Liang MN, Batyuk A, Koglin JE, Carbajo S, Boutet S, Moriarty NW, Holton JM, Dobbek H, Adams PD, Bergmann U, Sauter NK, Zouni A, Messinger J, Yano J, Yachandra VK (2018) Structures of the intermediates of Kok's photosynthetic water oxidation clock. Nature 563(7731):421–425. https://doi.org/10.1038/s41586-018-0681-2

Kim DH, Britt RD, Klein MP, Sauer K (1992) The manganese site of the photosynthetic oxygen-evolving complex probed by EPR spectroscopy of oriented photosystem II membranes: the $g = 4$ and $g = 2$ multiline signals. Biochemistry 31:541–547. https://doi.org/10.1021/bi00117a034

Kok B, Forbush B, McGloin M (1970) Cooperation of charges in photosynthetic O_2 evolution. Photochem Photobiol 11:457–476. https://doi.org/10.1111/j.1751-1097.1970.tb06017.x

Krewald V, Retegan M, Cox N, Messinger J, Lubitz W, DeBeer S, Neese F, Pantazis DA (2015) Metal oxidation states in biological water splitting. Chem Sci 6(3):1676–1695. https://doi.org/10.1039/c4sc03720k

Kulik LV, Epel B, Lubitz W, Messinger J (2007) Electronic structure of the Mn_4O_xCa cluster in the S_0 and S_2 states of the oxygen-evolving complex of photosystem II based on pulse ^{55}Mn-ENDOR and EPR spectroscopy. J Am Chem Soc 129:13421–13435. https://doi.org/10.1021/ja071487f

Li XC, Siegbahn PEM (2015) Alternative mechanisms for O_2 release and O-O bond formation in the oxygen evolving complex of photosystem II. Phys Chem Chem Phys 17(18):12168–12174. https://doi.org/10.1039/c5cp00138b

Li HJ, Nakajima Y, Nomura T, Sugahara M, Yonekura S, Chan SK, Nakane T, Yamane T, Umena Y, Suzuki M, Masuda T, Motomura T, Naitow H, Matsuura Y, Kimura T, Tono K, Owada S, Joti Y, Tanaka R, Nango E, Akita F, Kubo M, Iwata S, Shen JR, Suga M (2021) Capturing structural changes of the S_1 to S_2 transition of photosystem II using time-resolved serial femtosecond crystallography. IUCrJ 8:431–443. https://doi.org/10.1107/S2052252521002177

Lubitz W, Chrysina M, Cox N (2019) Water oxidation in photosystem II. Photosynth Res 142(1):105–125. https://doi.org/10.1007/s11120-019-00648-3

Messinger J (2004) Evaluation of different mechanistic proposals for water oxidation in photosynthesis on the basis of Mn_4O_xCa structures for the catalytic site and spectroscopic data. Phys Chem Chem Phys 6:4764–4771. https://doi.org/10.1039/B406437B

Messinger J, Badger M, Wydrzynski T (1995) Detection of *one* slowly exchanging substrate water molecule in the S_3 state of photosystem II. Proc Natl Acad Sci USA 92:3209–3213. https://doi.org/10.1073/pnas.92.8.3209

Navarro MP, Ames WM, Nilsson H, Lohmiller T, Pantazis DA, Rapatskiy L, Nowaczyk MM, Neese F, Boussac A, Messinger J, Lubitz W, Cox N (2013) Ammonia binding to the oxygen-evolving complex of photosystem II identifies the solvent-exchangeable oxygen bridge (μ-oxo) of the manganese tetramer. Proc Natl Acad Sci USA 110(39):15561–15566. https://doi.org/10.1073/pnas.1304334110

Nilsson H, Krupnik T, Kargul J, Messinger J (2014a) Substrate water exchange in photosystem II core complexes of the extremophilic red alga *Cyanidioschyzon merolae*. Biochim Biophys Acta 1837(8):1257–1262. https://doi.org/10.1016/j.bbabio.2014.04.001

Nilsson H, Rappaport F, Boussac A, Messinger J (2014b) Substrate-water exchange in photosystem II is arrested before dioxygen formation. Nat Commun 5:4305. https://doi.org/10.1038/ncomms5305

Pantazis DA (2018) Missing pieces in the puzzle of biological water oxidation. ACS Catal 8(10):9477–9507. https://doi.org/10.1021/acscatal.8b01928

Pantazis DA, Ames W, Cox N, Lubitz W, Neese F (2012) Two interconvertible structures that explain the spectroscopic properties of the oxygen-evolving complex of photosystem II in the S_2 state. Angew Chem Int Ed 51(39):9935–9940. https://doi.org/10.1002/anie.201204705

Pushkar Y, Ravari AK, Jensen SC, Palenik M (2019) Early binding of substrate oxygen is responsible for a spectroscopically distinct S_2 state in photosystem II. J Phys Chem Lett 10(17):5284–5291. https://doi.org/10.1021/acs.jpclett.9b01255

Rapatskiy L, Cox N, Savitsky A, Ames WM, Sander J, Nowaczyk MM, Rögner M, Boussac A, Neese F, Messinger J, Lubitz W (2012) Detection of the water-binding sites of the oxygen-evolving complex of photosystem II using W-band ^{17}O electron-electron double resonance-detected NMR spectroscopy. J Am Chem Soc 134(40):16619–16634. https://doi.org/10.1021/Ja3053267

Schuth N, Zaharieva I, Chernev P, Berggren G, Anderlund M, Styring S, Dau H, Haumann M (2018) K alpha X-ray emission spectroscopy on the photosynthetic oxygen-evolving complex supports manganese oxidation and water binding in the S_3 state. Inorg Chem 57(16):10424–10430. https://doi.org/10.1021/acs.inorgchem.8b01674

Shevela D, Kern JF, Govindjee G, Messinger J (2023) Solar energy conversion by photosystem II: principles and structures. Photosynth Res 156(3):279–307. https://doi.org/10.1007/s11120-022-00991-y

Siegbahn PEM (2009) Structures and energetics for O_2 formation in photosystem II. Acc Chem Res 42(12):1871–1880. https://doi.org/10.1021/Ar900117k

Siegbahn PEM (2013) Substrate water exchange for the oxygen evolving complex in PSII in the S_1, S_2, and S_3 states. J Am Chem Soc 135(25):9442–9449. https://doi.org/10.1021/ja401517e

Suga M, Akita F, Hirata K, Ueno G, Murakami H, Nakajima Y, Shimizu T, Yamashita K, Yamamoto M, Ago H, Shen JR (2015) Native structure of photosystem II at 1.95 Å resolution viewed by femtosecond x-ray pulses. Nature 517(7532):99–103. https://doi.org/10.1038/nature13991

Suga M, Akita F, Sugahara M, Kubo M, Nakajima Y, Nakane T, Yamashita K, Umena Y, Nakabayashi M, Yamane T, Nakano T, Suzuki M, Masuda T, Inoue S, Kimura T, Nomura T, Yonekura S, Yu LJ, Sakamoto T, Motomura T, Chen JH, Kato Y, Noguchi T, Tono K, Joti Y, Kameshima T, Hatsui T, Nango E, Tanaka R, Naitow H, Matsuura Y, Yamashita A, Yamamoto M, Nureki O, Yabashi M, Ishikawa T, Iwata S, Shen JR (2017) Light-induced structural changes and the site of O=O bond formation in PSII caught by XFEL. Nature 543(7643):131–135. https://doi.org/10.1038/nature21400

Suga M, Akita F, Yamashita K, Nakajima Y, Ueno G, Li HJ, Yamane T, Hirata K, Umena Y, Yonekura S, Yu LJ, Murakami H, Nomura T, Kimura T, Kubo M, Baba S, Kumasaka T, Tono K, Yabashi M, Isobe H, Yamaguchi K, Yamamoto M, Ago H, Shen JR (2019) An oxyl/oxo mechanism for oxygen-oxygen coupling in PSII revealed by an x-ray free-electron laser. Science 366(6463):334–338. https://doi.org/10.1126/science.aax6998

Tagore R, Chen HY, Crabtree RH, Brudvig GW (2006) Determination of μ-oxo exchange rates in di-μ-oxo dimanganese complexes by electrospray ionization mass spectrometry. J Am Chem Soc 128(29):9457–9465. https://doi.org/10.1021/ja061348i

Tagore R, Crabtree RH, Brudvig GW (2007) Distinct mechanisms of bridging-oxo exchange in di-μ-O dimanganese complexes with and without water-binding sites: implications for water binding in the O_2-evolving complex of photosystem II. Inorg Chem 46(6):2193–2203. https://doi.org/10.1021/ic061968k

Tanaka A, Fukushima Y, Kamiya N (2017) Two different structures of the oxygen-evolving complex in the same polypeptide frameworks of photosystem II. J Am Chem Soc 139(5):1718–1721. https://doi.org/10.1021/jacs.6b09666

Umena Y, Kawakami K, Shen JR, Kamiya N (2011) Crystal structure of oxygen-evolving photosystem II at a resolution of 1.9 Å. Nature 473(7345):55–61. https://doi.org/10.1038/Nature09913

Vassiliev S, Zaraiskaya T, Bruce D (2012) Exploring the energetics of water permeation in photosystem II by multiple steered molecular dynamics simulations. Biochim Biophys Acta 1817(9):1671–1678. https://doi.org/10.1016/j.bbabio.2012.05.016

Vinyard DJ, Brudvig GW (2017) Progress toward a molecular mechanism of water oxidation in photosystem II. Annu Rev Phys Chem 68(1):101–116. https://doi.org/10.1146/annurev-physchem-052516-044820

Vinyard DJ, Ananyev GM, Dismukes GC (2013) Photosystem II: the reaction center of oxygenic photosynthesis. Annu Rev Biochem 82:577–606. https://doi.org/10.1146/annurev-biochem-070511-100425

Vinyard DJ, Khan S, Brudvig GW (2015) Photosynthetic water oxidation: binding and activation of substrate waters for O-O bond formation. Faraday Discuss 185:37–50. https://doi.org/10.1039/c5fd00087d

Vinyard DJ, Khan S, Askerka M, Batista VS, Brudvig GW (2017) Energetics of the S_2 state spin isomers of the oxygen-evolving complex of photosystem II. J Phys Chem B 121(5):1020–1025. https://doi.org/10.1021/acs.jpcb.7b00110

Wang J, Armstrong WH, Batista VS (2021) Do crystallographic XFEL data support binding of a water molecule to the oxygen-evolving complex of photosystem II exposed to two flashes of light? Proc Natl Acad Sci USA 118(24):e2023982118. https://doi.org/10.1073/pnas.2023982118

Yachandra VK, Sauer K, Klein MP (1996) Manganese cluster in photosynthesis: where plants oxidize water to dioxygen. Chem Rev 96:2927–2950. https://doi.org/10.1021/cr950052k

Yamaguchi K, Miyagawa K, Shoji M, Isobe H, Kawakami T (2022a) Elucidation of a multiple S_3 intermediates model for water oxidation in the oxygen evolving complex of photosystem II. Calcium-assisted concerted O-O bond formation. Chem Phys Lett. https://doi.org/10.1016/j.cplett.2022.140042

Yamaguchi K, Shoji M, Isobe H, Kawakami T, Miyagawa K, Suga M, Akita F, Shen JR (2022b) Geometric, electronic and spin structures of the $CaMn_4O_5$ catalyst for water oxidation in oxygen-evolving photosystem II. Interplay between experiments and theoretical computations. Coord Chem Rev. https://doi.org/10.1016/j.ccr.2022.214742

Young ID, Ibrahim M, Chatterjee R, Gul S, Fuller FD, Koroidov S, Brewster AS, Tran R, Alonso-Mori R, Kroll T, Michels-Clark T, Laksmono H, Sierra RG, Stan CA, Hussein R, Zhang M, Douthit L, Kubin M, de Lichtenberg C, Pham LV, Nilsson H, Cheah MH, Shevela D, Saracini C, Bean MA, Seuffert I, Sokaras D, Weng TC, Pastor E, Weninger C, Fransson T, Lassalle L, Brauer P, Aller P, Docker PT, Andi B, Orville AM, Glownia JM, Nelson S, Sikorski M, Zhu DL, Hunter MS, Lane TJ, Aquila A, Koglin JE, Robinson J, Liang MN, Boutet S, Lyubimov AY, Uervirojnangkoorn M, Moriarty NW, Liebschner D, Afonine PV, Waterman DG, Evans G, Wernet P, Dobbek H, Weis WI, Brunger AT, Zwart PH, Adams PD, Zouni A, Messinger J, Bergmann U, Sauter NK, Kern J, Yachandra VK, Yano J (2016) Structure of photosystem II and substrate binding at room temperature. Nature 540(7633):453–457. https://doi.org/10.1038/nature20161

Zimmermann JL, Rutherford AW (1984) EPR studies of the oxygen-evolving enzyme of photosystem II. Biochim Biophys Acta 767(1):160–167. https://doi.org/10.1016/0005-2728(84)90091-4